Non-invasive Pressure Measurement in PVC Tube

Richard Metslaid

Master's thesis
2018:E3

LUND UNIVERSITY

Faculty of Engineering
Centre for Mathematical Sciences
Mathematics

CENTRUM SCIENTIARUM MATHEMATICARUM

Non-invasive pressure measurement in PVC tube

Richard Metslaid
Supervisors: Hans Bengtsson and Kalle Åström

February 28, 2018

Abstract

In peritoneal dialysis it is important to make sure the pressure doesn't exceed certain limits. It is desirable to do the measuring without inserting anything inside of the tubing containing the dialysate.
This project uses a load cell pressed against the outside of the PVC tubing to estimate the pressure inside. The interval tested is approximately atmospheric pressure ±220 mBar. The temperature is constant room temperature ($\approx 20^o$C). The best estimate of the pressure uses a neural network to process the data and results in a mean absolute error of 7.31 mBar. The max error is 126 mBar. The target accuracy was ≈ 20 mBar and approximately 88.6 % of the errors are below or equal to 20 mBar. Unfortunately the errors are highly autocorrelated so there is a possibility of something missing from the model.

Acknowledgements

I would like to thank my supervisors Kalle Åström and Hans Bengtsson for helping me during the whole project, especially for keeping me on path and focusing on the important parts.
I would also like to thank Johan Andersson for discussions and being helpful with a lot of different things during the project.
Finally, I want to thank everyone else at Triomed AB for taking time and helping me whenever asked, providing everything needed and being generally encouraging.

Contents

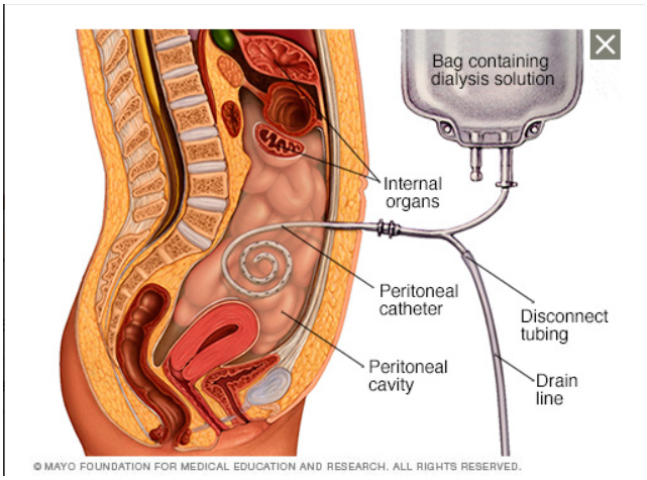

Figure 1: Illustration of the setup for Peritoneal dialysis. Image from the Mayo foundation for medical education and research [10].

1 Introduction

1.1 Background, problem formulation and purpose

Triomed AB (triomed.se) is developing a portable dialysis machine. It uses a dialysis technique called peritoneal dialysis [22]. In peritoneal dialysis the peritoneum (a membrane in the stomach) is used as a filter to remove for example urea from the blood. A tube is operated into the patient on one end, and connected to the dialysis machine on the other end. The purpose of the tube is to transport the fluids. In figure 1 an illustration is shown. During peritoneal dialysis it is important to make sure that the pressure inside the tubing to the peritoneum is neither too high nor too low. The fluids are not transported solely by gravity, but by a pump and some form of control system is necessary.

When pressure in a liquid is to be measured, a common approach is to have a membrane between the liquid and the reactive material (such as a capacitor). This adds an additional part that needs to be changed probably as frequently as the rest of the tubing, increasing costs. If the pressure could be measured in a non-invasive way, it could reduce this cost and possibly improve usability.

The purpose of this project is to find and/or develop a method that can measure the pressure in a (predefined) PVC tube containing water at room temperature. Ideally it should not require modifications to the tubing or too frequent calibration (more often than every 5 minutes). The major difference from the standard presure sensors is that since no modifications to the tubing are allowed, the measuring needs to be non-invasive. It is however allowed to be

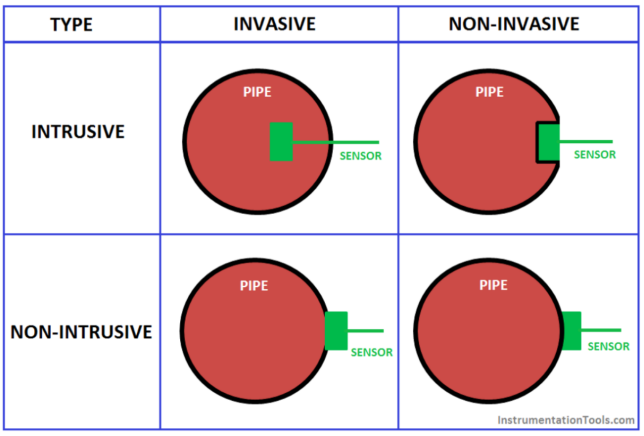

Figure 2: Illustration of the different ways to apply a sensor. Image from InstrumentationTools.com [24]

intrusive. An illustration of the difference is shown in figure 2

The resolution that is aimed for is 20 mBar. Finally, the final apparatus cannot be too large, heavy or expensive (loosely defined).

1.2 Current methods

1.2.1 Sensors for pressure measuring

There are multiple different ways to measure pressure. The method chosen generally depend on the requirements for accuracy, the circumstances under which the measuring will take place, and the environment. The prerequisite for methods covered here will be that they are non-invasive. If a membrane or other modification to the tube is allowed, this project would need major changes since there are already several methods and sensors developed for this kind of more "ordinary" pressure evaluations.

In the case with a membrane, the pressure can be known to great precision since there is direct contact with the medium. If it is to be done from outside the tube, a proxy for the pressure inside the tube has to be used. The most obvious proxy is the expansion or contraction of the tube.

One way to measure the pressure non-invasively is to press a force-sensor (load cell) against the outside of the tube. In a recent article [26] they attempted to measure the pressure on a model of a bone. The pressure was changed by applying calibrated weights. They tested several different force-sensors. Unfortunately the tests did not cover underpressures and the dynamics were fairly limited but overall it seemed successful. So using a force sensor seems possible. A commercially available product that appears to have similar application is

provided by Tekscan [28] [29]. It is unclear how accurate it is and appear to only recognize increases in pressure.

One potential way would be to optically measure the pressure change. There are very accurate photoelectric sensors on the market, for example Micro-Epsilon sells a product that measures film thickness (usually plastic sheets) using a photoelectric sensor and through-beam technology. They achieve an accuracy of approximately $3\mu m$ [19]. They also have a triangulation sensor with accuracy that's approximately the same. The downside to these methods are mainly that they are bulky and expensive. The same arguments regarding bulkiness and cost applies to microscopy and interferometry.

An ordinary camera could be possible to use, given that it is possibile to detect features (eg. edge detection) on sub-pixel level, for an explanation of theory and example, see [15] and [14]. This is discussed more in *Optical possibilities for measuring strain*.

If modifications to the outside of the tube was to be allowed, there are a few more possibilities. It could be worth investigating how a strain gauge performed if it was attached to the surface of the tube. Depending on how sensitive the gauge was (and considering what type of adhesive is used) it could be a good solution.
There is also some research on attaching a capsule filled with oil directly to the outside of the tube and having a fiber optic pressure sensor inside the capsule [11]. When the pressure inside the tube changes, the oil would also experience a change in pressure and this would be captured by the fiber optic sensor.

If one can change a part of the tube and add a membrane, an ordinary camera could be a plausible solution. This was tested in a recent article [21].

1.2.2 Transforming or mapping data

Given that some form of measurement with a sensor has taken place, it needs to be converted to a unit that we can interpret. Generally there will go a current through the sensor and the size of the output current changes depending on the value measured. So the readings need to be converted (in this case to pressure and mBar) and possible noise etc. should be removed as well as possible.

There are several different methods available. For this report, these can be divided into parametric and non-parametric regression methods.
Parametric methods basically imply that the parameters of the model doesn't change when the size of the dataset does see [17]. An example of this are the ordinary Least squares (often used to fit a line or a plane to a set of points). If a non-parametric regression method is used, the parameters for the model usually increase with increased training data. An example of this is Kernel regression or a weighted average.

However, this is not always a very important distinction to make. For example, if a Neural network is used, it can be either parametric or not depending on how it is implemented.

If the data needs to be normalized there are several different ways to do this. If the training data comes from a known distribution, it is often a good idea to use the normalization

$$x_n = \frac{x - \mu}{\sigma}, \tag{1}$$

where x_n is the normalized x, μ and σ are the mean and standard deviation of the distribution. This can be used when one wants to compare data of distributions with different means etc.
If the distribution is not known and the importance perhaps rather lies in simplifying future applications, feature scaling can be used. This requires the minimum and maximum values to be known, and the data is rescaled to $[0, 1]$. The formula

$$x_n = \frac{x - x_{min}}{x_{max} - x_{min}}, \tag{2}$$

can be modified to rescale the data to other intervals too, if that would be more appropriate. The paper [25] has a section more fully covering different aspects of normalization.

1.3 Tube parameters

The calculations below are to provide a general context and approximation of how sensitive the method or sensor type that is chosen needs to be.
The tube is assumed to be made of plasticized PVC. This means that the Young's modulus (a material constant to measure stiffness with unit Pascal) lies somewhere between approximately 20 MPa and 2.5 GPa [3] [1] [2].
The alternative would be silicone rubber, which has a Young's modulus between approximately 1 MPa and 50 MPa [4]. For silicone rubber it's assumed that the tubing potentially replacing the PVC is in the upper (more stiff) range.

The outer diameter of the tube is approximately 5 mm, yielding a outer radius of 2.5 mm. The inner radius is approximately 1.5 mm.
The length is assumed to be infinite so that effects on the edge can be ignored. This is reasonable since the pressure will be measured where the tube will be fairly straight, meaning that it will not bend or end in the close vicinity.

1.3.1 Simplistic model for the tubes deformation

To find the strain at the outer edge of the tube we use Hooke's law and Lamé's equations (a good explanation is given in [9]) for thick-walled cylinders (pressure vessels). This is because the strains are assumed to be so small that the

deformations are linear. We can't use the equations for thin walls since the tube is too thick. The relationship between the radial- and hoop-stresses are

$$\begin{aligned} \sigma_r &= A - \frac{B}{r^2}, \\ \sigma_c &= A + \frac{B}{r^2}, \end{aligned} \tag{3}$$

where σ_r and σ_c are the radial- and hoop-stresses in the tube. Here, A and B are constants and r is the radius. The strain in the circumferential direction is then given by

$$\epsilon_c = \frac{1}{E}(\sigma_c - v\sigma_r), \tag{4}$$

where E is Young's modulus and v Poisson's ratio. The strain is generally defined as

$$\epsilon = \frac{newC - oldC}{oldC} = \frac{2\pi(r+\delta) - 2\pi r}{2\pi r} = \frac{\delta}{r}. \tag{5}$$

1.3.2 Example of the tubes expansion

The boundary values for the problem are that inside the tube there is a constant pressure of +2kPa (+20 mBar). So the radial stress on the inner wall is -2000 Pa. On the outer wall there is no radial stress. So $\sigma_r(0.0015) = -2000$ and $\sigma_r(0.0025) = 0$. This gives us

$$\begin{aligned} -2000 &= A - \frac{B}{0.0015^2}, \\ 0 &= A - \frac{B}{0.0025^2}, \end{aligned} \tag{6}$$

which after solving the system yields: $A = 1125$ and $B = 0.007$. Inserting this into the equation for σ_c we get

$$\sigma_c(0.0025) = 1125 + \frac{0.007}{0.0025^2} = 2245\text{Pa}. \tag{7}$$

The value of E that will be used is 45 MPa. As a lower softness-threshold this is reasonable when the alternative for the tubing, silicone rubber is considered and noticing that the actual PVC used is likely not the softest PVC possible. Now we use equation (4) to find the strain

$$\epsilon_c = \frac{1}{45 \cdot 10^6} \cdot (2245 - 0) = 4.9889 \cdot 10^{-5}. \tag{8}$$

The radius was 0.0025 m, so this gives a $\delta = 4.9889 \cdot 10^{-5} \cdot 0.0025 = 1.2472 \cdot 10^{-7} m$. This is the change in radius, which is 0.00012472 mm.

1.3.3 Optical possibilities for measuring strain

It is interesting to know if a camera could be used. A review article covering different available optical methods was published in 2009 [5] (that article covers more than just ordinary cameras).
It is assumed the field of view is 1 dimensional and that the field of view is 6 mm (since the tube is five and it expands a little bit).
If the radius increases by 0.00012472 mm the diameter would increase by 0.00024944 mm. If there was no, or a only a very small amount of processing available this would mean that the resolution necessary was given by

$$\text{resolution} = \frac{6}{0.00024944} = 24054 \text{ pixels.} \tag{9}$$

This is fairly unreasonable, especially considering that the field of view for the camera will generally be much larger than 6 mm if all the pixels are to be used.

However, it is possible to approximate on sub-pixel level, and measuring the size is essentially an edge-detection problem. If the required amount of pixels could be lowered by a couple of magnitudes, it would be a clearly viable option. The image processing needs to be able to detect edges with an accuracy of a few magnitudes higher precision than the amount of pixels.
This is not unreasonable, see for example [18] and [6]. However, it does seem like a difficult approach to implement compared to the force sensor (load cell) which seems promising.

1.4 Limitations of the project

Some limitations are stated in *Background, problem formulation and purpose*. Others include that only one type of PVC tubing is used and the temperature is constant ($\approx 20^oC$). The pressure span of interest is approximately -220 mBar (-22 kPa) to +220 mBar (+22 kPa). The target resolution is approximately $\pm$20 mBar ($\pm$2 kPa). It will be assumed that the pressure is at atmospheric level when the measuring starts. The changes in pressure are assumed to be fairly slow and not impulse-like (time-scale for changes will be of several seconds). Furthermore, continuous calibrations are allowed.

2 Method

2.1 Set-up

Given the importance of not modifying the tube, a standard force-sensor (FS20 Low Force Compression Load Cell - Measurements Specialities) is the sensor used (unless an other type of equipment is deemed necessary).

The tube is placed on top of the sensor and inside a socket so that the tube is pre-stressed. The pre-stressing is to make negative pressure measurable. The

design of the socket is discussed in the subsection *Socket for the force-sensor*.

Behaviour of the force-sensor will be tested using different training cycles where the pressure is known. These cycles have different lengths, where the longest are approximately 4 hours. Over the cycle the pressure varies between $\approx \pm 220$ mBar. A reference pressure sensor is used to measure the actual pressure.

These cycles will be used as training data for a model to predict the pressure given the data from the force sensor when the reference pressure sensor is not used.

The mapping between force and pressure is done continuously and different methods are compared. Generally, the mean value of the absolute error will be minimized rather than max-error or any other type.

2.2 Material

The physical material used are:

- Arduino Uno with breadboard and cables.
- Oina Peristaltic pump.
- Servo controller ESCON Module 24/2.
- FS20 low force compression load cell.
- Power supply, providing ≈ 15 V.
- PVC tubing with accessories.
- Bowl for water and a sealable bin acting as pressure vessel.
- Socket for clamping the sensor and tube, with screws.
- Double sided adhesive tape.
- Supportive frame.
- Reference pressure sensor.
- Handheld pressure sensor.
- Hand powered pump.

The software used to control the Arduino is the standard Arduino IDE.
The servo controller was configured with ESCON studio.
Processing of the data and creation of graphs etc. was done in Matlab.

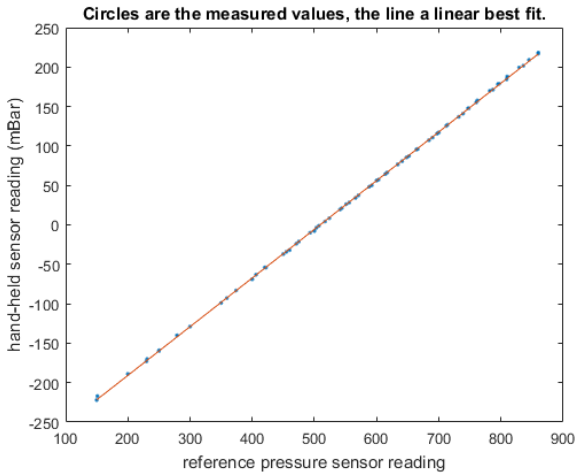

Figure 3: The data on how the reference pressure sensor is scaled to mBar units.

2.3 Reference pressure sensor

The reference pressure sensor is assumed to be accurate and linear enough for the application. The reference pressure sensor is calibrated with a handheld pressure sensor (values noted by hand) that is also assumed to be accurate enough. The linearity and accuracy of the reference is important as it will be assumed to be a key value for all of the following calculations. The best-fit of the reference sensor and hand-held device is shown in figure 3. The line is given by:

$$\text{reading} \cdot 0.6174 - 314.2632 = \text{pressure}[mBar]. \tag{10}$$

2.4 Force-sensor

The sensor used is Measurements Specialities - FS20 Low Force Compression Load Cell. It spans 0-750 grams force [27]. It is shown, with a part of the tubing for reference, in figure 4.

Problems with its accuracy (which would be a combination of non-linearity, hysteresis and repeatability) is stated in the specifications sheet [27] and presumed small compared to the hysteresis, non-linearity and repeatability resulting from the actual system with the tube and the socket. However, the resolution of the sensor given the magnitude of the pressure changes could be a limiting factor. This can be seen in figure 5. Using a handheld pressure sensor and a hand powered pump, the relationship between measured force and pressure was measured. Since the pressure span is ≈ 440 mBar totally and the force readings span ≈ 70, the resolution can most likely not be better than ≈ 6.3 mBar. That is without considering noise and variance.

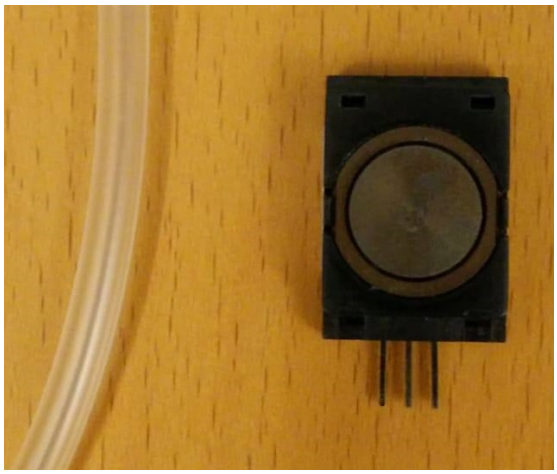

Figure 4: Sensor and tube. The tube has a diameter of ≈ 5 mm.

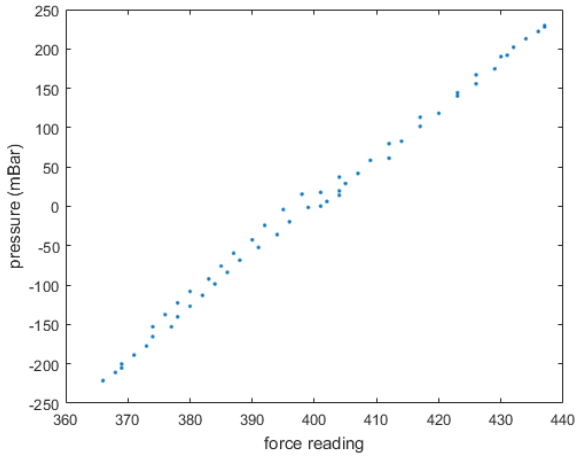

Figure 5: Relationship between force measured and pressure inside the tube. Note that each value pair has been allowed to stabilize.

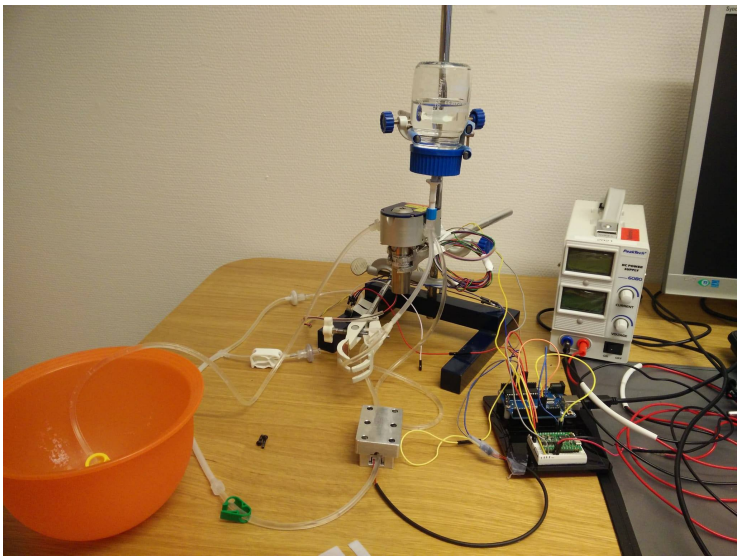

Figure 6: The configuation used with the final choice of socket.

2.5 Socket for the force-sensor

The socket will encapsulate the sensor and part of the tubing, with the purpose of fixating the tube across the middle of the sensors top part. The socket also creates a pre-stress that allows for measuring of pressures below 0 mBar. 3D models of the socket are created in CAD with the help of Stefan Landholm and Hans Bengtsson. Prototypes are printed in a 3D printer.
The major factors of consideration are:

- How much should the pre-stress be?
- How is it made sure that the pre-stress is constant?
- What shape should the socket have?

2.6 Test apparatus

A set up to try different configurations and general testing was built. It consisted of tubing, peristaltic pump, pressure vessel (a jar with lid and seal) and a bowl of water. The pump was controlled by an Arduino Uno with a breadboard and a servo controller, ESCON Module 24/2 [20]. An additional power supply was also used (the pump requires more than the 5 voltage the Arduino provides). Both the force- and pressure-sensor were controlled by the Arduino and readings were logged in the console. The final set up is shown in figure 6.

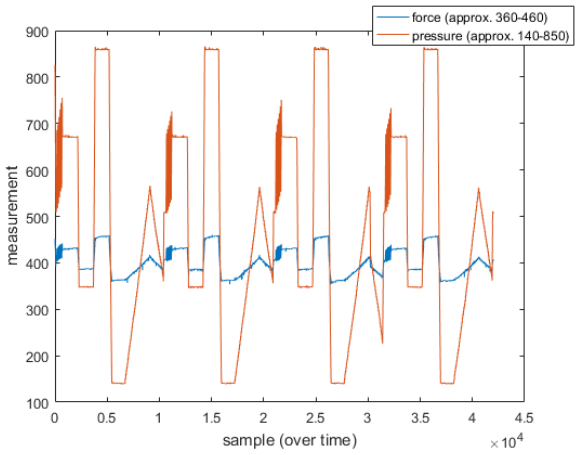

Figure 7: Example of a cycle. The real pressure spans between approximately -220 mBar and +220 mBar. There are a couple of different speeds and levels with constant pressure

2.7 Choice of test cycles

The test cycles were designed to contain the full span of the pressure range and to cover different dynamics in the changes of pressure (rapid and slow changes both up and down, constant low pressure and constant high pressures etc.). Measurements were printed to the console every 0.2 seconds. Figure 7 shows an example of just over 2 hours of measuring. In figure 8 a part of figure 7 is magnified to show details.

3 Mapping force to pressure

3.1 General considerations

There were three methods used. The first is a polynomial fit and the second uses a neural network to find the pressure. Kernel regression is also attempted. In all cases processing of the training data is required (can be done offline).

There is also a reference model that convert the force to pressure. This is to find out whether further processing is actually worth doing (for example the neural network takes substantial time to train, the Kernel regression requires a lot of memory). The force is scaled using the data that is shown in figure 5. The scaling factor, given that data, with a linear best fit is ≈ 6.206.
The 0 mBar level is found from the calibrations. Since there is clearly a lot of drift in the beginning of a cycle, when only one calibration takes place the first

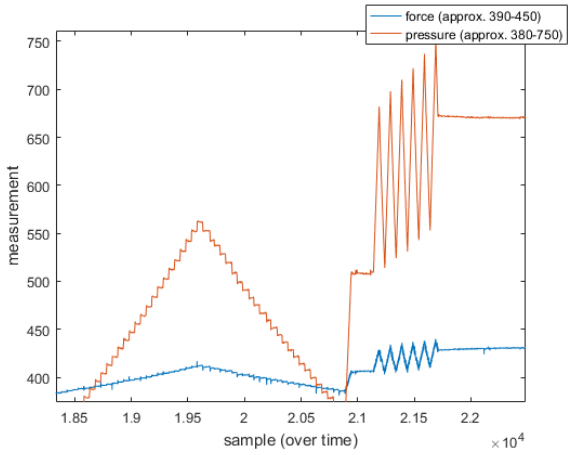

Figure 8: Close-up of a part of figure 7. Notice the similarities between the force and the pressure but also how the force doesn't change as much as the pressure.

10 minutes are removed and not considered.

Methods that require more than rescaling all share some major considerations. These are:

- Removing the drift/relaxation of the tube present after clamping it in the socket.
- Finding what the max- and min-values of the force are given the pressure conditions.
- Mapping each force-reading, or a transformation of a force reading, to a pressure value.

The drift is a large problem and is not shown in figure 7. That is because that cycle is recorded so long after the initial clamping that the residuals are (presumably) gone. The effects of the drift are easier to see in figure 9. The cycle is just under 4 hours.

The max- and min-values for the force vary from cycle to cycle (despite it being the same cycle) so a way to estimate the boundaries is necessary. Figure 10 shows a couple of examples of another cycle where the conditions of the measuring has been made as similar as (realistically) possible (same place on the tube each cycle, temperature controlled, waiting before starting a new cycle etc.). The initial variation is from clamping the socket. Part of correcting this is simply translating and cropping the data. In figure 11 the first 300 samples (1 min) are removed and the initial force reading is translated to equal 0. The variance of the measured force between the samples is clearly visible in figure

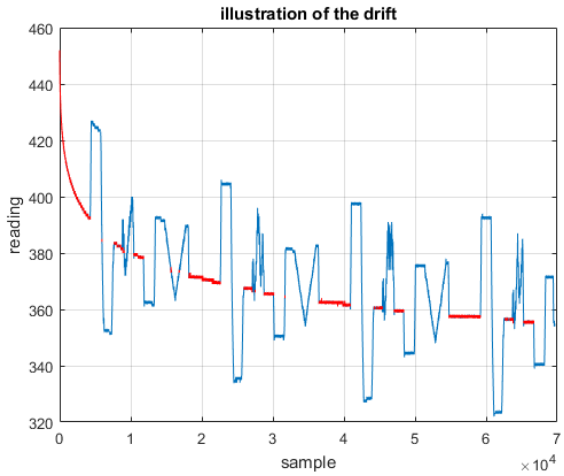

Figure 9: The cycle started less than a minute after clamping the tube. The red parts are all representing atmospheric pressure. Total time shown almost 4 hours.

11. Considering the resolution of the sensor (see the subsection *force-sensor*) this is not negligible.

After the data is scaled, translated, etc. (pre-processed) the actual mapping can be done in several different ways. The three main methods tested are:

- Polynomial regression using Matlab's $fit()$.
- Kernel regression, with the Gaussian kernel, implemented separately.
- Neural network, using Matlab's built in *nntraintool*.

3.2 Least squares

Given the data points x (which would be the force measured) and the key values y (the reference pressure) and the assumption of a second degree polynomial as a relationship, we minimize

$$min(z)_{a_1,a_2,a_3} = \sum_{i=1}^{N}(y - a_1 \cdot x^2 - a_2 \cdot x - a_3)^2. \tag{11}$$

If the relationship is assumed to be linear, then a_1 is set to 0. For this, Matlab's function $fit(x, y, 'type')$ is used. If the relationship is of an other form (ex. $y = a_1 \cdot e^{a_2 \cdot x} + a_3$) the same minimization problem applies.
For more information on Least squares, the article [30] provides a good explanation.

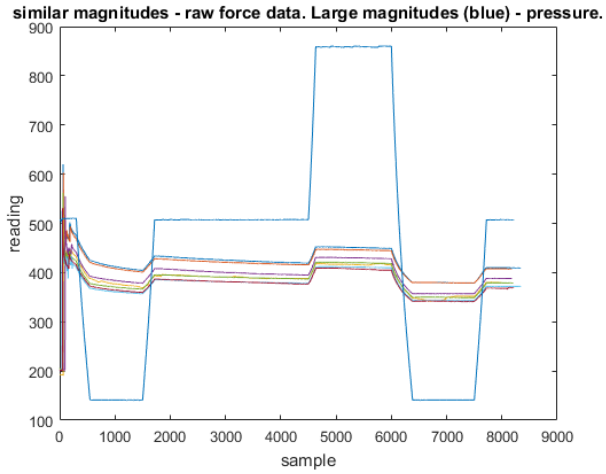

Figure 10: Raw data to illustrate normal variance. Total time shown around 25 minutes.

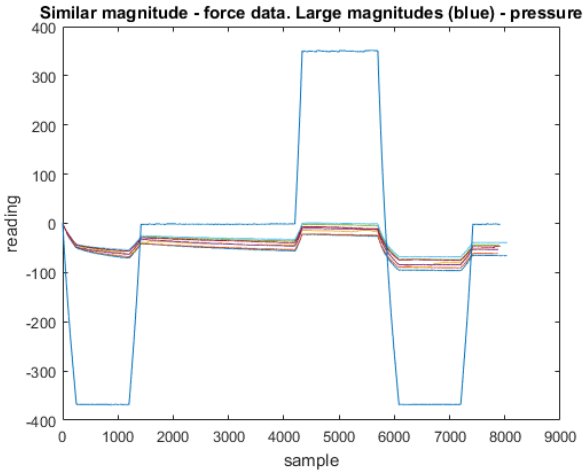

Figure 11: Raw pressure data and translated force data to illustrate minimal variance. Total time shown around 25 minutes.

3.3 Kernel regression

Kernel regression is a non-parametric method of estimation, meaning that there are not as strict conditions on the underlying function as with for example a linear fitting method. The specific method used here is the Nadaraya-Watson kernel estimator, named after the inventors [8] [12]. It is presented below:

$$f(x_0) = \frac{\sum_{i=1}^{N} y_i \cdot K_h(x_i, x_0)}{\sum_{i=1}^{N} K_h(x_i, x_0)}, \tag{12}$$

where $f(x_0)$ is the function estimation (the pressure) for the value x_0 and $K(x_i, x_0)$ is the kernel. In this report, the Gaussian kernel will be used so

$$K(x_i, x_0) = e^{(\frac{x_i - x_0}{h})^2}, \tag{13}$$

where h is the bandwidth and to be chosen depending on sample size and what the level of smoothing should be (larger h means more smoothing). Note that there is usually a normalizing term but it cancels out. Things to note is that the kernel is even and that normalization is necessary. The normalization is done by rescaling the data to the interval $[0, 1]$. For the training data this is done exactly for each training set. For the test data, the mean min- and max-values from the training data are used and values that end up outside the bounds are mapped to the respective boundary. Since the estimation is based on an average, the training data should be uniform to not create a bias [23].

3.4 Neural network

For a training set x and key values y Matlab's already implemented neural network is used. First an initial net is created with $net = fitnet(amountOfLayers)$ and then it is trained by $trainedNet = train(net, x, y)$.

The Levenberg-Marquardt algorithm [16] [7] is used. The method finds the minimum to the function

$$F(z) = 0.5 \sum_{i=1}^{N} (f_i(z))^2 \tag{14}$$

by creating a matrix with the Jacobians to $f_i(z)$ and doing certain modifications to the Gauss-Newton method, the updating scheme is

$$z_{i+1} = z_i - (J^T(z_i)J(z_i) + \mu_i I)^{-1} J^T(z_i) f(z_i), \tag{15}$$

where μ is a parameter to allow invertability, and

$$J(x) = \begin{bmatrix} \frac{\delta f_1(z)}{\delta z_1} & \frac{\delta f_1(z)}{\delta z_2} & \dots & \frac{\delta f_1(z)}{\delta z_N} \\ \frac{\delta f_2(z)}{\delta z_1} & \dots & & \\ \dots & & \dots & \\ \frac{\delta f_N(z)}{\delta z_1} & \dots & & \frac{\delta f_N(z)}{\delta z_N} \end{bmatrix}, \tag{16}$$

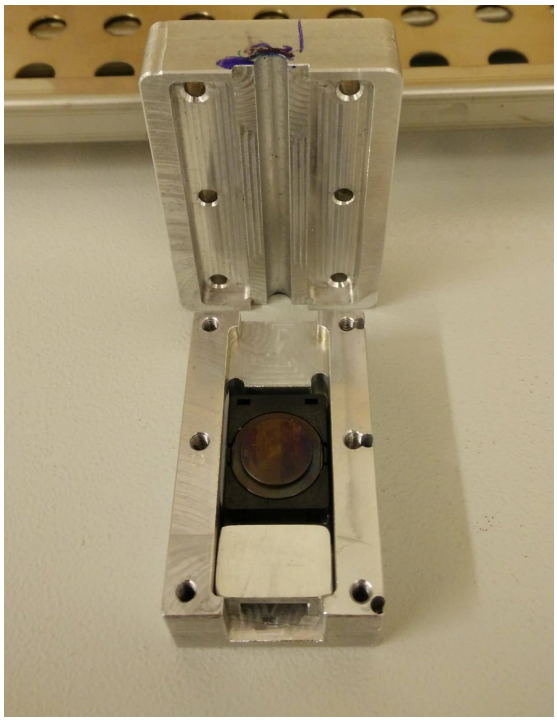

Figure 12: Final socket and the force sensor.

where z are the parameters we want to find [31]. A good explanation is given in [13].

4 Result

4.1 The socket

The final version of the socket is made of aluminium with holes for screws. It is shown in figure 12. The tube is placed in the groove in the lid (shown standing) and then placed on top of the bottom part with the force sensor inside. The aluminium provides a constant distant between the lid and the sensor which appear to be independent from how hard the screws are fastened. This was not the case with a plastic socket (that had to be clamped/pinned instead of screwed in place).

4.2 Pressure from the reference model

When there is only one calibration taking place, the first 10 minutes are removed and then the calibration takes place. the mean absolute error is ≈ 181 mBar.

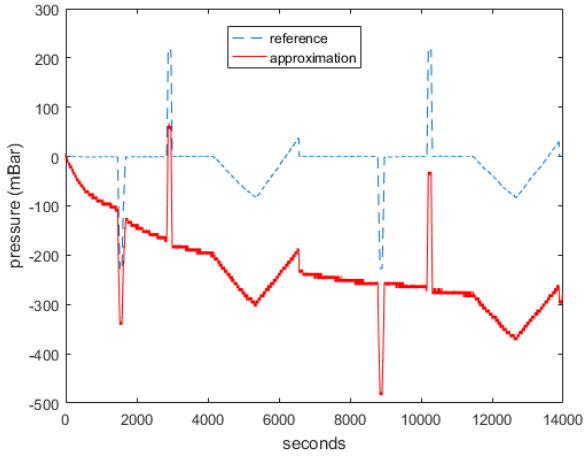

Figure 13: The blue (upper) is the reference pressure. the red (lower) is the calculated pressure. Almost 4 hours shown, 1 calibration.

The max error is ≈ 302 mBar. An example fit is shown in figure 13.
When more calibrations are allowed, only the first minute is removed. The calibrations are done at minutes: 0, 9, 17, 50, 67 or 77 depending on what cycle is used and, if possible, also at 120 and 183 minutes.
The mean absolute error is ≈ 24.7 mBar and the max error ≈ 223 mBar. The same raw data as in figure 13, is shown in figure 14 but with the additional calibrations.

4.3 Pressure from other models

4.3.1 Training data, drift and calibration

Approximately the first minute of the data is removed. The calibrations are done at the same places as for the reference case (so 0, 9, 17, 50, 67 or 77 and if possible 120 and 183 minutes).

Given continuous measuring, the drift removal is a constant function approximated by

$$g(t) = a_1 \cdot e^{a_2 \cdot t} + a_3 \cdot e^{a_4 \cdot t}, \tag{17}$$

where a_1, a_2, a_3, a_4 are the average parameter values from the training data. The parameters were found using all parts of the training data where the pressure was atmospheric, and fitted using Matlab's $fit(x, y, 'exp2')$. An example of a cycle before and after subtraction of $g(t)$ is shown in figure 15. The training data has its drift removed and the actual fit to the data is used. An example of the modified force and key pressure values, after drift removal, are shown in figure 16.

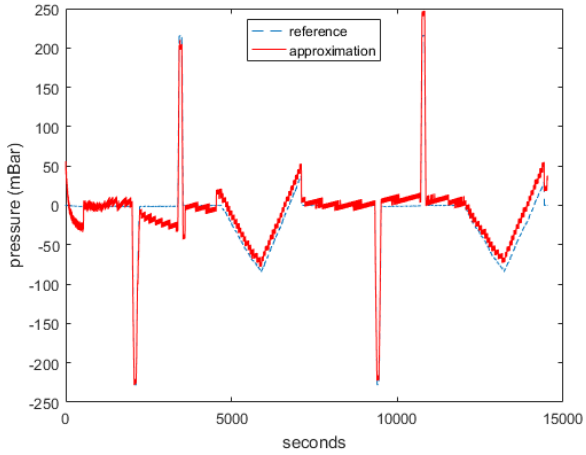

Figure 14: The blue (dashed line) is the reference pressure. the red (solid) is the calculated pressure. Almost 4 hours shown, 7 calibrations.

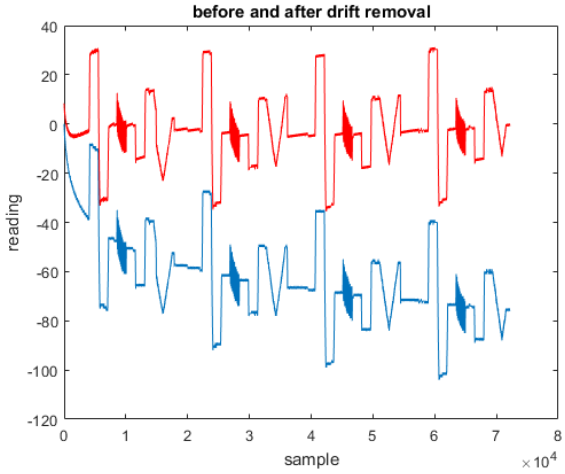

Figure 15: The blue (lowest part) is before drift removal. The red (top part) after drift removal.

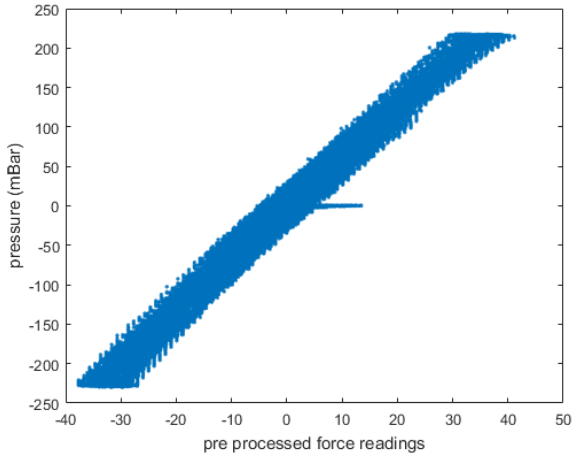

Figure 16: Reference pressure data and pre-processed force data. Note that there's a remaining variance in force for a certain pressure.

4.3.2 Polynomial fit

A second degree polynomial fit, where the polynomial parameters are the mean parameters from the training data, gives a mean absolute error of ≈ 10.8 mBar and a max error of ≈ 120 mBar.
An example of parameters for the function are

$$\text{pressure [mBar]} = -0.0157 \cdot (\text{force reading})^2 + 6.644 \cdot (\text{force reading}) - 1.7969 \tag{18}$$

This provided a slight improvement compared to a first order fit. Example fits are shown in figure 17 and figure 18. The mapping is shown in figure 19.
If only one calibration was used (and the 10 first minutes removed instead of just 1), the mean absolute error was ≈ 24.2 mBar and the max error ≈ 148 mBar.

4.3.3 Kernel regression fit

The Gaussian kernel was used with a bandwidth of 0.006. The bandwidth was found by trial and error. The mean absolute error was ≈ 11.1 mBar and the absolute error ≈ 113 mBar. Example fits are shown in figure 20 and in figure 21. The mapping is shown in figure 22.
If only one calibration was used (and the 10 first minutes removed instead of just 1), the mean absolute error was ≈ 21.1 mBar and the max error ≈ 163 mBar.

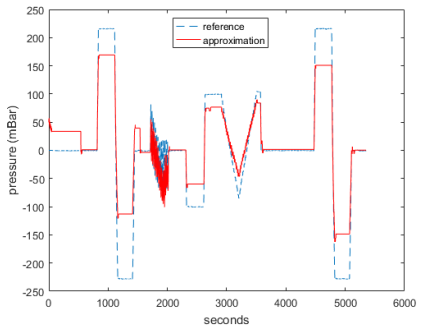

Figure 17: Example of poor performance from the polynomial fit.

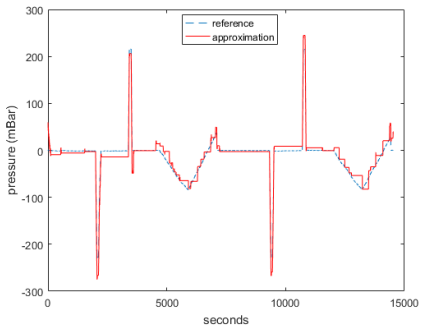

Figure 18: Example of good performance from the polynomial fit.

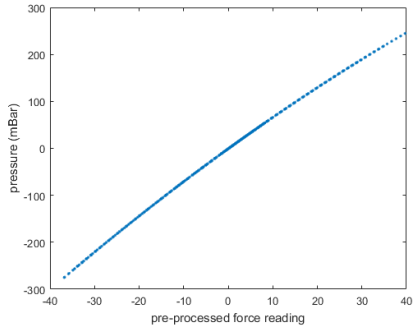

Figure 19: Mapping from force to pressure for the polynomial fit.

4.3.4 Neural network fit

Using a neural net with a Levenberg-Marquardt algorithm and 25 hidden layers provided a mean absolute error of ≈ 7.28 mBar and a max error of ≈ 126 mBar. If 10 layers were used, the performance was lowered slightly but the speed of training was faster. An example fit is shown in figure 23 and also in figure 24. The mapping is shown in figure 25.
If only one calibration was used (and the 10 first minutes removed instead of just 1), the mean absolute error was ≈ 35.5 mBar and the max error ≈ 296 mBar. This was with 10 layers instead of 25 (25 layers yielded a mean absolute error of ≈ 49.4 mBar)

4.3.5 Comparison between methods

There are other parameters except the mean absolute error and the max-error that can be used to evaluate the methods. Table 1 shows a couple of measurements to simplify comparison. The reference is the one with the same amount of calibrations as the other methods (more than 1).

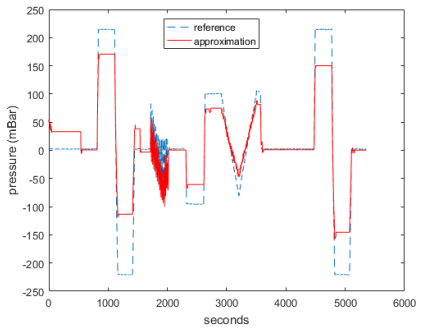

Figure 20: Example of poor performance from the Kernel regression.

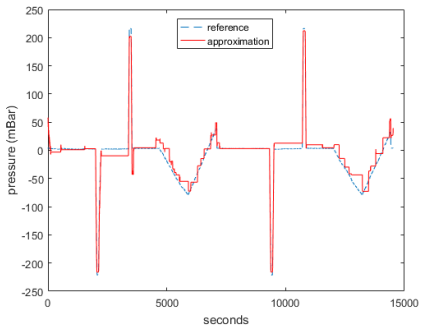

Figure 21: Example of good performance from the Kernel regression.

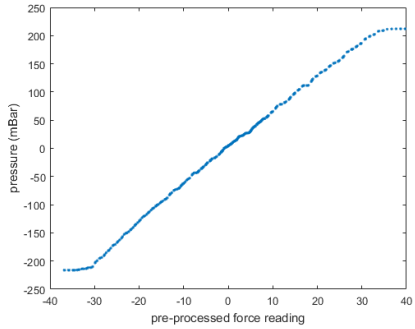

Figure 22: Mapping from force to pressure with Kernel regression.

Note that the correlation between the error and pressure (in the last row) is calculated on the actual error values. If the absolute error is used, the correlations change. For the polynomial fit the correlation increases to -0.1658, while the Neural network fit and the Kernel regression fit both see lowered correlations, -0.09 and -0.14 respectively. The reference pressure correlation is lowered to 0.0467.

5 Discussion

5.1 The sensor and design of the socket

5.1.1 General discussion of the workflow

The socket went through several iterations. The lids depth didn't seem to make a noticeable difference as long as it kept the tube properly in place (the amount of pre-stress did not appear important). The first models didn't do this and

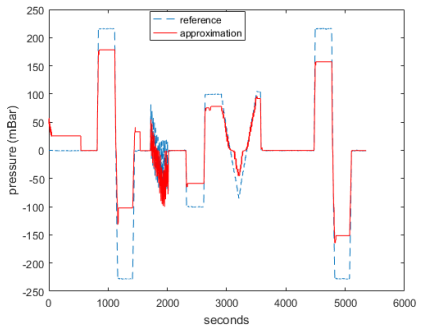

Figure 23: Example of poor performance from the neural network.

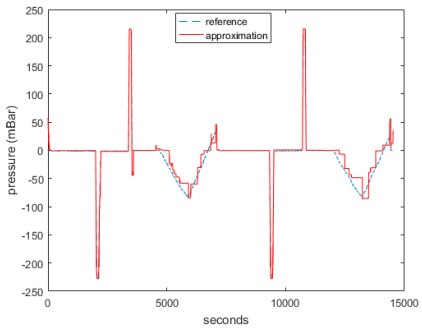

Figure 24: Example of good performance from the neural network.

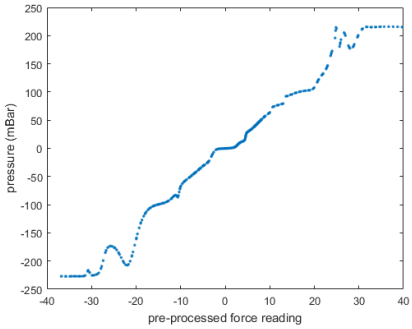

Figure 25: Mapping from force to pressure with the Neural network.

are shown in figure 26. With hindsight it is fairly obvious why the first two models/lids are insufficient; they allow too much movement of the tube. The argument for using a non-round shape was that it might affect how the tube expanded in a negative way (eg. increasing friction).

Before the third lid is evaluated, it is worth reiterating what the socket is supposed to do. The tube that the measurement is done upon can and will be removed and put back during the lifetime of the sensor and socket. This is a important part since a large benefit of non-invasive measuring is that the sensor and socket can be kept while the tube is exchanged. While there almost always will be some difference between different tubes, it could improve accuracy to have all external factors as similar as possible.

The problem with the third iteration of the lid to the socket is that there is no good way to create a proper pre-stress. The edges of the bottom part to the socket are narrow in comparison to the lid so the top part (lid) is allowed to bend and relax considerably depending on how much force is applied to keep

	Reference	Polynomial	Neural network	Kernel regression
Mean absolute error	24.7	10.8	7.31	11.1
Max absolute error	223	120	126	113
% of errors >20 mBar	40.0	15.0	11.4	14.7
% of errors >50 mBar	12.5	0.98	1.25	0.92
Error and pressure correlation	0.17	-0.02	0.20	0.24

Table 1: Comparison between mapping methods

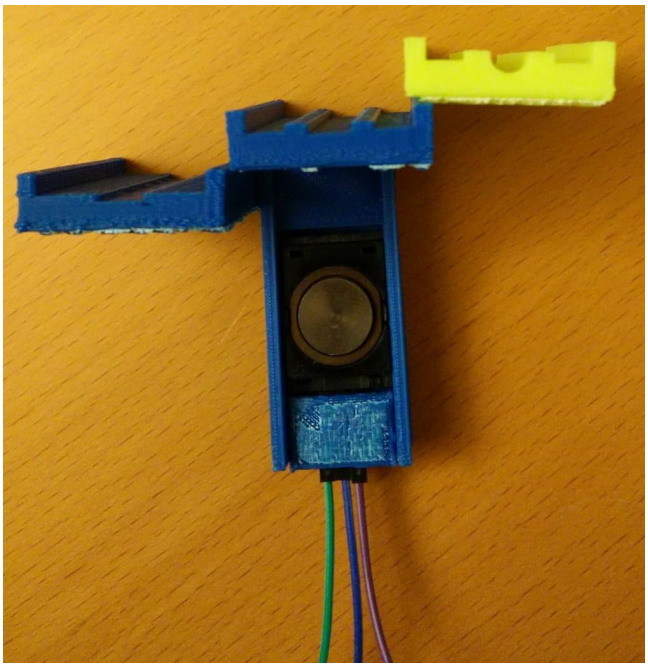

Figure 26: First lid to the left, second middle and third to the right.

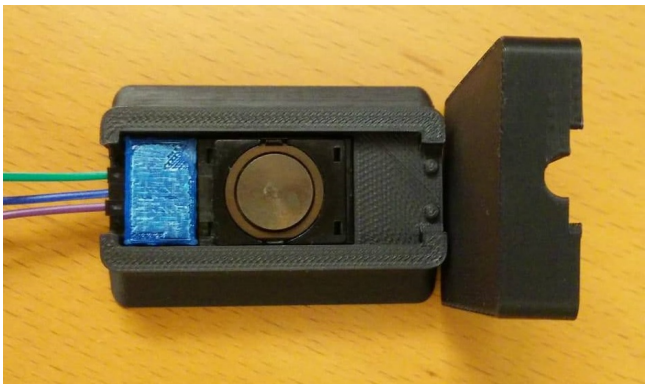

Figure 27: Fourth attempt for the socket.

it closed (kept close by putting a heavy box of sand on top). As long as the difference is not too extreme (values going out of sensor bounds) this can be handled by calibration. However, it is probably not increasing the accuracy. The fourth model, shown in figure 27, are made of a more rigid plastic and generally thicker.
This socket is good. Unfortunately the box of sand used to keep the lid closed is large relative to the lid, and moves easily. This cause variance in the pre-stress and hence in the measuring. For the final version of the socket, it was realized (by Hans Bengtsson) that the defining part of the pre-stress is that the distance between the lid and bottom part should be the same, independent of the external force applied. Hence the final version of the socket was designed (made in CAD by Stefan Landholm) in aluminium and with holes for screws so the reliance on the sand box was removed. It is shown in figure 12. It is worth noting that the sensor itself is attached to the socket by double-coated adhesive tape.

5.1.2 Possible improvements, physical parameters

It could help to have a more clip-on type of closure for the lid. It would be easier and could possibly reduce residuals from the attachment of the screws.

The resolution from the sensor is fairly low and it could probably increase accuracy to have a more sensitive force-sensor.

Considering the decreased drift when a silicone tube was used instead of a PVC tube (*Limitations of the result*) a change to silicone tubing could also improve performance.

If the force sensor was replaced with a camera (discussed as an option previously), the initial drift could maybe be removed if it is assumed that it stems

from the clamping. It would be quite likely that one would have to deal with other problems instead, but if the need for calibrations was removed that would be a large benefit.

5.2 The models and the errors

5.2.1 General accuracy

From table 1 we see that the best average error comes from the mapping using a Neural network. However, all three methods perform quite similarly with the majority of the errors being smaller than 20 mBar.
The very large errors ($>$ 100 mBar) are unfortunate and appear to take place when the pressure changes rapidly and the change in diameter is delayed.

While the average mean absolute error is generally low if the calibrations are done, there are some other concerning aspects.

One part is that the min- and max-vales are not only different, but that the difference between the max- and the min-value ($max_{forceReading} - min_{forceReading}$) changes. There is no good explanation to this yet. Part of it might come from variance in placement of the tube, maybe even from how hard the lid is screwed even though it was assumed negligible.
It could also come from the sensor itself. This is at least probably part of the reason. The sensors accuracy is stated as an unknown combination of non linearity, hysteresis and repeatability and is $\pm 1\%$ of the span. Since 1% of the span is enough to change the output by more than 1 reading, this could result in a noticeable change in the mapping to pressure.

5.2.2 The error

The error is not randomly distributed but rather correlated to itself. This is especially true within a given cycle. In figures 28-31, the autocorrelation of the mean absolute average errors are shown for the reference fit, the kernel regression fit, the polynomial fit and the neural network fit respectively. Note that the maximal lag of a 100 samples correspond to 20 seconds.

The large correlation is a bad feature. If it was low and the real pressure constant, averaging the estimation would approach the actual average. Now that is not the case.

The neural network fit appears to result in slightly less correlation but it is still quite significant. It is unclear why it performs better. The other methods are fairly similar.

One reason for the large correlation is probably that the pressure is constant for relatively long amounts of time, causing the force reading to also be fairly

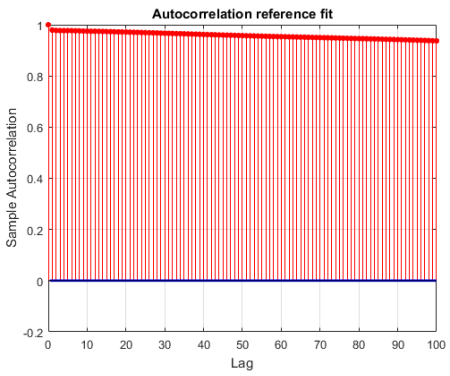

Figure 28: Autocorrelation between errors for the reference fit.

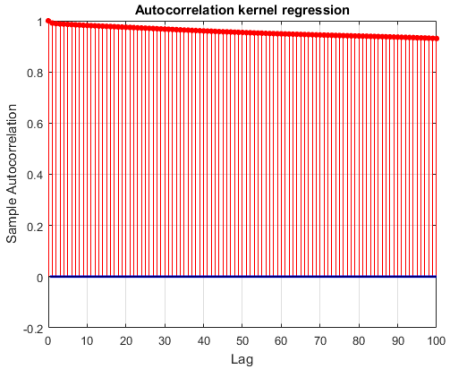

Figure 29: Autocorrelation between errors for the kernel regression fit.

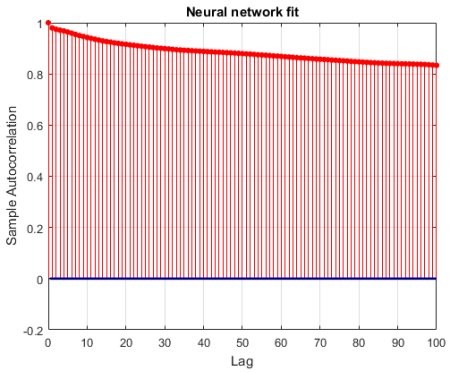

Figure 30: Autocorrelation between errors for the neural network fit.

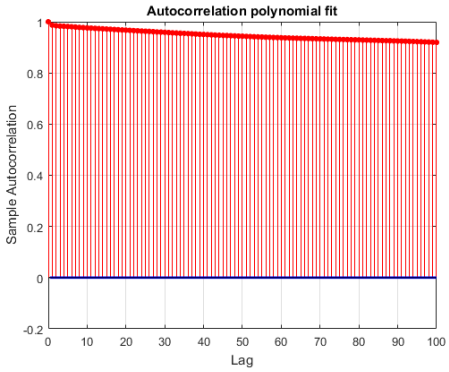

Figure 31: Autocorrelation between errors for the polynomial fit.

constant. That means that the mapping wont change. However, that doesn't explain why the mapping is not accurate.

A reasonable explanation to the autocorrelation of the error and the error itself could be the delay between a pressure change and the time for the tube to adapt its size. If this is the case, an increase in error and a large change of pressure would be fairly correlated (or close to ± 1).
The derivative of the pressure is approximated by first averaging with a filter of size 100 (using Matlab's $movmean()$), then calculating the difference between these elements using $diff()$ and zero-padding at the end. The interesting part is the absolute change (both increases and decreases in pressure), so the absolute value is calculated.
The derivative of the error is found in the exact same way. As can be seen in table 2, the correlation coefficients are fairly large. The conclusion is that the

Source of error	correlation
Error from reference	0.23
Error from kernel regression	0.50
Error from polynomial fit	0.51
Error from neural network	0.54

Table 2: Correlations between the estimated derivatives of the errors and the estimated derivatives of the pressure.

delay could potentially be a part of the reason for the errors autocorrelation.

Generally, if the error is not white noise or can't be approximated as such the conclusion would be that the model lack something. There could for example be some parameter missing. This might be the case, especially considering that the correlation between different models errors are fairly large (for example the correlation coefficient between the polynomial fit error and the neural network fit error is 0.82). Another hypothesis (so not the delay) is that the larger changes in pressure induce new drift that is not as noticeable as the one from the clamping, but large enough to not be negligible.

5.2.3 Possible improvements of the mapping

It is clear that frequent calibrations are very important. It seems very likely that the accuracy will increase if the frequency is increased further. However, it also seems as the longer a cycle goes on, the less frequent the calibrations needs to be. The initial drift is mostly gone after a couple of hours.
The frequency for the calibrations was chosen with this in mind. Unfortunately, the use of calibrations came in rather late in the project so the majority of the cycles had already been recorded and wouldn't allow for calibrations at totally arbitrary times (and since there would be no realistic way to calibrate at, for example, 200 mBar it wasn't tested).

It could be an idea to approximate the pressure using not one method but a combination. Unfortunately the errors between the different methods are fairly correlated so the accuracy isn't really improved.

Another idea is to not map the force directly to the pressure, but instead modify or transform the force and then map this or these values to the pressure. for example the square root, or using both the force and some of the previous values to take the history into account. Several variations of this was tested and it didn't seem to give any substantial improvement, except for a slightly smaller max-error in a few cases.

5.3 Limitations of the result

5.3.1 Parameters from the set-up

An important limitation is that the softness of the tube is impacted by the surrounding temperature. If the temperature decreases the tube stiffens and will most likely change diameter slower. On the other hand, if the temperature increases the tube softens and probably expands or contracts faster. A cold temperature has no clear benefits what so ever, a warmer temperature will probably lower the amount of drift so if it is accounted for it could possibly improve the measurements.

Another factor that was briefly examined was how the dynamics would be with a tube made out of silicone instead of PVC. The hypothesis was that a silicone tube would have less drift since the material is more flexible.
In figure 32 and figure 33, the only modifications to the recorded data are that the first minute has been removed and the cycles have all been translated so they are the same at the start. There are approximately 25 minutes shown. The reference pressure for all of the individual cycles, both for PVC and silicone, are shown in figure 34.
A potential source of error is that the silicone tube has a slightly smaller diameter than the PVC tube so the range used for measuring on the force sensor is slightly different. There is, however, nothing from the previous tests and measurements that would suggest that this would cause the difference in performance.
It seems clear from figure 34 that the pressure is basically the same for all the cycles, no matter whether the tube was PVC or silicone.
It also seems clear that the PVC (figure 32) exhibits more drift and also a larger variance, compared to the silicone (figure 33).

5.3.2 Parameters from the mapping

The interval over which the measuring takes place is well defined and one would have to be careful to extrapolate the result to outside of the boundaries. For the polynomial model, there is a possibility that the method is worth using a little bit outside of the bounds. The second degree polynomial provided only a slight improvement over the first degree so it is reasonable to assume that it wouldn't be useless. For the neural network and especially the kernel regression, it is important to have training data for the very majority of the possible results (ex. the kernel regression output NaN's out of bounds, or if there's a large gap in the data).

5.4 Other sources of error

Since a breadboard was used, a large part of the cables weren't soldered. If they moved or was in some way disturbed, this caused large amount of noise.
Similarly, if the force sensor was not fixed but allowed to move, this caused

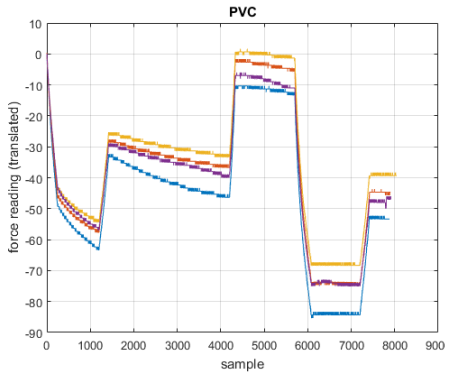

Figure 32: 4 short cycles using a PVC tube.

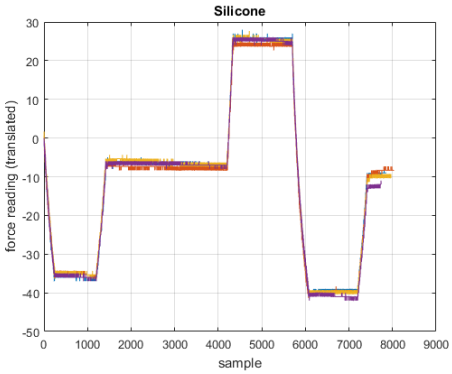

Figure 33: 4 cycles using a silicone tube.

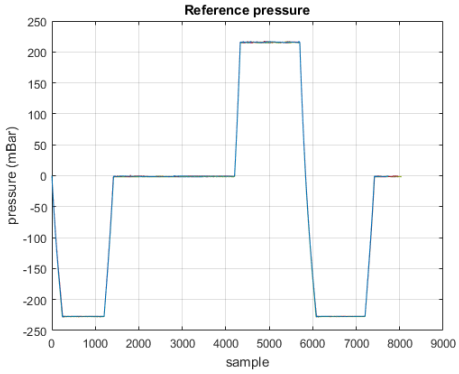

Figure 34: Actual reference pressures for the PVC and silicone comparison.

large changes (usually drops) when it moved. Because of this, it was made sure that everything was fairly stable and not moving during tests. However, there is probably still a little noise stemming from movement.
The longest cycle tested was just above 4 hours. The drift seems to approach 0 (realized after keeping the tube pre-stressed over night and then used for testing) but if longer cycles are to be used, it might be worth increasing the length of the training cycles too.
Figure 35 illustrates both a cycle after a long pre-stress, and the noise caused by movement in the cables. The full cycle is just below 2.5 hours. The reference pressure is shown in figure 36.

Another thing worth considering is the sampling speed. The readings are printed every 0.2 seconds and this was chosen simply because it appeared to be a good compromise between fast enough to capture changes, but not so fast that the

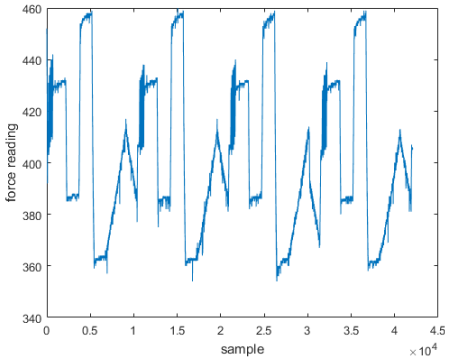

Figure 35: Force readings after letting the tube sit in the socket over night.

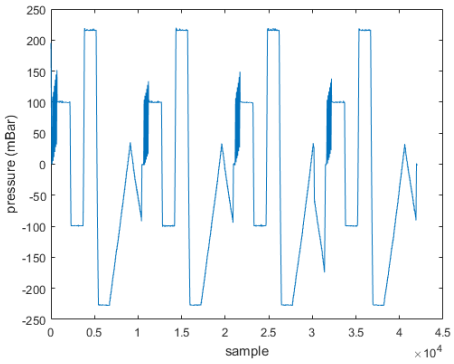

Figure 36: Reference pressure to figure 35.

sheer amount of data for training cycles would be hindering. It is possible that reduced sampling speed could improve memory requirements. It is uncertain if increased sample speed would result in any benefits given the current environment.

6 Conclusion

The purpose of this report was to find a way of measuring the pressure in a PVC tube without creating any changes to said tubing. The result relies upon the temperature being kept constant at (close to) 20^oC, frequent calibrations (although not more often than every 9 minutes) and sufficient training data being available.

If a combination of calibration and a neural network is used the mean absolute error is < 8 mBar and approximately 88.6% of the measurements have error less than or equal to 20 mBar (which was stated target resolution).
Unfortunately there might be something missing from the model used since the error is autocorrelated and the reliance on frequent calibrations is not optimal.

It is important that the socket used to connect the tube and sensor is rigid and consistent with the pre-stress it creates.
The choice of sensor could probably be improved since it doesn't need to cover such a large span as it currently does.

References

[1] Pvc soft. *https://www.matbase.com/material-categories/natural-and-synthetic-polymers/thermoplastics/commodity-polymers/material-properties-of-soft-polyvinyl-chloride-soft-pvc.html#properties*.

[2] Pvc soft - pvc-p. *http://www.designerdata.nl/plastics/thermo+plastics/PVC+soft+-+PVC-P*.

[3] Pvc strength. *http://www.pvc.org/en/p/pvc-strength*, 2017.

[4] AZoM.com. Silicone rubber. *https://www.azom.com/properties.aspx?ArticleID=920*, 2001.

[5] H.Xie A.Asundi B.Pan, K.Qian. Two-dimensional digital image correlation for in-plane displacement and strain measurement: a review. *Measurement Science and Technology*, 20(6), 2009.

[6] C.Steger. Evaluation of subpixel line and edge detection precision and accuracy. *https://pdfs.semanticscholar.org/747d/a551860576f511775b0842580becfed4ada3.pdf*, 1998.

[7] D.W.Marquardt. An algorithm for least-squares estimation of nonlinear parameters. *Journal of the Society for Industrial and Applied Mathematics*, 11(2):431441, 1963.

[8] E.A.Nadaraya. On estimating regression. *Theory of Probability & Its Applications*, 9(1):141–142, 1964.

[9] Paul E.Labossiere. Thick walled cylinders. *http://courses.washington.edu/me354a/Thick%20Walled%20Cylinders.pdf*.

[10] Mayo foundation for medical education and research. Peritoneal dialysis. *https://www.mayoclinic.org/tests-procedures/peritoneal-dialysis/about/pac-20384725*, 2017.

[11] T.Pustelnya & A.Gacekb & P.Gibinskib & R.Kustoszc G.Konieczny a &, Z.Opilskia &. Results of experiments with fiber pressure sensor applied in the polish artificial heart prosthesis. *Acta Physica Polonica A*, 118(6):http://przyrbwn.icm.edu.pl/APP/PDF/118/a118z6p24.pdf, 2010.

[12] G.S.Watson. Smooth regression analysis. *The Indian Journal of Statistics*, 26(4):359–372, 1964.

[13] M.T.Hagan & H.B.Demuth & M.H.Beale & O. De Jesus. Neural network design. *Martin Hagan*, 2nd edition:12–19 – 12–27, 2014.

[14] Anders Heyden Kalle Åström. Stochastic modelling and analysis of sub-pixel edge detection. *http://www2.maths.lth.se/vision/publdb/reports/pdf/astrom-heyden-icpr-96.pdf*, 1996.

[15] Anders Heyden Kalle Åström. Stochastic analysis of image acquisition, interpolation and scale-space smoothing. *http://www2.maths.lth.se/vision/publdb/reports/pdf/astrom-heyden-aap-99.pdf*, 1999.

[16] K.Levenberg. A method for the solution of certain non-linear problems in least squares. *Quarterly of Applied Mathematics*, 2(2):164–168, 1944.

[17] Hamdy Mahmoud. Parametric versus semi/nonparametric regression models. *Virginia Tech, Department of Statistics*, http://www.lisa.stat.vt.edu/?q=node/7517, 2014.

[18] P.Kulla M.Hagara. Edge detection with sub-pixel accuracy based on approximation of edge with erf function. *Radioengineering*, 20(2), 2011.

[19] Micro-epsilon. https://www.micro-epsilon.se/measurement-systems/kunststoff-inspektion/tiefziehextrusion/. 2017.

[20] Maxon motor. Escon module 24/2 servo controller. *https://www.maxonmotor.com/maxon/view/news/MEDIARELEASE-ESCON-MODULE-24-2-EN-COM*, 2014.

[21] Krzysztof Murawski. New vision sensor to measure gas pressure. *Measurement Science Review*, 15(3), 2015.

[22] The National Institute of Diabetes, Digestive, and Kidney Diseases Health Information Center. Peritoneal dialysis. *https://www.niddk.nih.gov/health-information/kidney-disease/kidney-failure/peritoneal-dialysis*.

[23] P.Breheny. Local regression 1. *University of Kentucky*, http://web.as.uky.edu/statistics/users/pbreheny/621/f12/notes/11-1.pdf, 2012.

[24] S.Bharadwaj Reddy. Difference between invasive & non-invasive and intrusive & non-intrusive. *https://instrumentationtools.com/difference-invasive-non-invasive-intrusive-non-intrusive/#.WmxRtoJzKpo*.

[25] R.M.Haralick S.Aksoy. Feature normalization and likelihood-based similarity measures for image retrieval. *Pattern Recognition Letters*, 22(5):563–582, 2001.

[26] O.Troynikov S.Parmar, I.Khodasevych. Evaluation of flexible force sensors for pressure monitoring in treatment of chronic venous disorders. *Sensors*, 17(8), 2017.

[27] Measurement Specialties. Fs20 low force compression load cell. *http://www.mouser.com/ds/2/418/FS20-709917.pdf*, 2011.

[28] Tekscan. https://www.tekscan.com/applications/infusion-pump-occlusion-detection. 2017.

[29] Tekscan. https://www.tekscan.com/applications/medical-device-evaluation. 2017.

[30] Eric W Weisstein. Least squares fitting. *MathWorld–A Wolfram Web Resource*, http://mathworld.wolfram.com/LeastSquaresFitting.html.

[31] Eric W Weisstein. Levenberg-marquardt method. *MathWorld–A Wolfram Web Resource*, http://mathworld.wolfram.com/Levenberg-MarquardtMethod.html.

Master's Theses in Mathematical Sciences 2018:E3
ISSN 1404-6342

LUTFMA-3338-2018

Mathematics
Centre for Mathematical Sciences
Lund University
Box 118, SE-221 00 Lund, Sweden

http://www.maths.lth.se/